Available online at www.sciencedirect.com
ScienceDirect
Journal of Photochemistry and Photobiology A: Chemistry 188 (2007) 245–251
Journal of Photochemistry and Photobiology A:Chemistry
www.elsevier.com/locate/jphotochem

Synthesis, crystal structure and photoluminescent behaviors of 3-(1H-benzotriazol-1-yl)-4-methyl-benzo[7,8]coumarin

Tianzhi Yu [a,*], Yuling Zhao [b], Xiansheng Ding [a], Duowang Fan [a], Long Qian [a], Wenkui Dong [b]

[a] *Key Laboratory of Opto-Electronic Technology and Intelligent Control (Lanzhou Jiaotong University), Ministry of Education, Lanzhou 730070, China*
[b] *School of Chemical and Biological Engineering, Lanzhou Jiaotong University, Lanzhou 730070, China*

Received 21 August 2006; received in revised form 22 November 2006; accepted 12 December 2006
Available online 16 December 2006

Abstract

A novel coumarin derivative containing an electron-transporting moiety (benzotriazole), 3-(1H-benzotriazol-1-yl)-4-methyl-benzo[7,8]coumarin (BMBC), was synthesized and characterized by element analysis, ^{1}H NMR, FT-IR and UV–vis absorption spectra, TG-DTA and single crystal X-ray crystallography. Crystallographic data reveal a dihedral angle of 60.4° between the benzocoumarin and benzotriazole rings, which is attributed to the spatial hindrance of a 4-positioned methyl group. The photoluminescent behaviors of BMBC doped in PMMA were discussed. The compound exhibits a strong blue emission under ultraviolet light excitation. The ground-state geometries, the lowest energy transition and the UV–vis spectrum of BMBC have been studied with density functional theory (DFT) and time-dependent density functional theory (TD-DFT) at B3LYP/6-31G(d) level, showing that the calculation outcomes are in good agreement with experimental data.

Keywords: Synthesis; Crystal structure; Photoluminescence; Coumarin derivative; UV–vis spectrum

1. Introduction

Coumarin and its derivatives occur widely in nature, and have been extensively exploited in biological, chemical and physical fields. Coumarins have outstanding optical properties, including an extended spectral range, high quantum yields, superior photostability and good solubility in common solvents, many natural and synthetic coumarin derivatives are widely used as laser dyes [1,2], nonlinear optical chromophores [3], fluorescent whiteners [4], as well as fluorescent labels and probes for physiological measurement [5–8]. Since Tang et al. [9] first used 3-(2-benzothiazolyl)-7-diehylaminocoumarin (coumarin 6) as a electroluminescent (EL) material successfully, coumarin derivatives have attracted much interest owing to their potential application in organic light-emitting diodes (OLEDs), many efforts have been devoted to explore new EL materials [10–12]. Coumarin derivatives are easily quenching in solid state, so as EL materials they were always doped in polymer host [9,13–15].

Recently, we synthesized a novel coumarin derivative, 3-(1-benzotriazole)-4-methyl-coumarin (BMC), by introducing an electron-accepting benzotriazole in 3-positions of the coumarin ring, which showed ultraviolet emission with a peak at 386 nm [16]. In this communication, we report the results for the synthesis, characterization and photoluminescent (PL) properties of a new coumarin derivative, 3-(1H-benzotriazol-1-yl)-4-methyl-benzo[7,8]coumarin (BMBC). We synthesized it in order to understand the effect of substituting the hydrogen of coumarin skeleton by groups on the photoluminescent properties of coumarin.

2. Experimental

2.1. Materials and methods

2-Acetyl-1-naphthol from Acros Organics and 1H-benzotriazole (BTA) from Aldrich were used without further purification. Chloroacetic acid and Phosphorus oxychloride were analytical grade reagents from Tanjin Fuchen Chemical Reagent Factory. Phosphorus oxychloride was dried and redistilled before using.

* Corresponding author. Tel.: +86 931 4956935; fax: +86 931 4956030.
E-mail address: ytz823@hotmail.com (T. Yu).

1010-6030/$ – see front matter © 2006 Elsevier B.V. All rights reserved.
doi:10.1016/j.jphotochem.2006.12.017

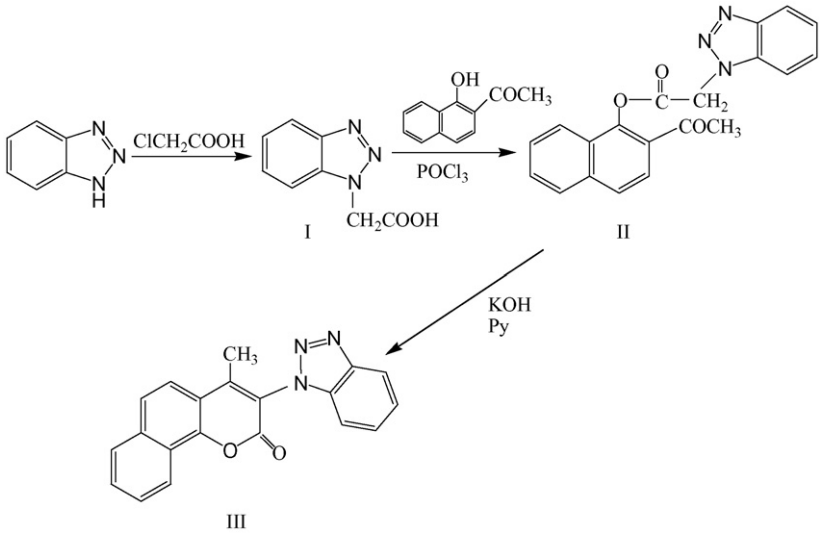

Scheme 1. Synthetic route of 3-(1H-benzotriazol-1-yl)-4-methyl-benzo[7,8]coumarin.

IR spectra (400–4000 cm^{-1}) were measured on a Shimadzu IRPrestige-21 FT-IR spectrophotometer. C, H, and N analyses were obtained using an Elemental Vario-EL automatic elemental analysis instrument. ^{1}H NMR spectra were obtained on Unity Varian-500 MHz. UV–vis absorption and fluorescence spectra were recorded on a Shimadzu UV-2550 spectrometer and on a Perkin-Elmer LS-55 spectrometer, respectively. The thermogravimetry (TG) and differential thermal analysis (DTA) were recorded on a Shimadzu DT-40 thermal analysis instrument. Melting points were measured by using a X-4 microscopic melting point apparatus made in Beijing Taike Instrument Limited Company, and the thermometer was uncorrected.

2.2. Synthesis and characterization of 3-(1H-benzotriazol-1-yl)-4-methyl-benzo[7,8] coumarin (BMBC)

The synthetic route was shown in Scheme 1.

2.2.1. (1-Benzotriazolyl) acetic acid (I)

It was synthesized from ^{1}H-benzotriazole and chloroacetic acid according to the method reported earlier [16].

2.2.2. (2-Acetyl) naphthol (1-benzotriazolyl) acetate (II)

Ten gram (0.0537 mol) of 2-acetyl-1-naphthol and 10.24 g (0.0578 mol) of (1-benzotriazolyl) acetic acid (I) were dissolved in 100 ml of dry pyridine. Then 6 ml of phosphorus oxychloride was added stepwise with magnetic stirring under 5–10 °C, and the mixture was stirred for 10 h at room temperature. After the reaction was complete, the mixture was poured into an aqueous solution of HCl containing fragment ice with vigorous stirring, and white precipitate was produced. The precipitate was filtered, and washed successively with diluted aqueous solution of $NaHCO_3$ (10%) and distilled water, respectively. After ethanol recrystallization, filtration and drying in vacuum, 13.71 g (74.0%) of white flocculent crystals was obtained. mp 166–168 °C. Anal. Calc. for $C_{20}H_{15}N_3O_3$ (%): C, 69.56; H, 4.38; N, 12.17. Found: C, 69.43; H, 4.61; N, 12.25. IR (KBr pellet, cm^{-1}): 1766 (ester C=O), 1676 (ketone C=O), 2991, 2953, 1466, 1357, 1185.

2.2.3. 3-(1H-benzotriazol-1-yl)-4-methyl-benzo[7,8]coumarin (III)

Into a one-neck, 100 ml round-bottomed flask were placed 6.9 g (0.02 mol) of (2-acetyl) naphthol (1-benzotriazolyl) acetate and 50 ml of dry pyridine, then 1.4 g (0.025 mol) of potassium hydroxide was added stepwise and the reaction mixture was stirred vigorously for 5 h at room temperature. After completing, the mixture was poured into the aqueous solution of HCl containing fragment ice with vigorous stirring, and primrose yellow precipitate was formed. Then the crude product was filtered and washed with distilled water, and purified with recrystallization from ethanol to yield 5.13 g (78.44%) of primrose yellow crystalline solid. mp 262–264 °C. Anal. Calc. for $C_{20}H_{13}N_3O_2$ (%): C, 73.38; H, 4.00; N, 12.84. Found: C, 73.05; H, 4.13; N, 12.37. IR (KBr pellet, cm^{-1}): 1727 ($\nu_{C=O}$). ^{1}H NMR (500 MHz, $CDCl_3$, δ, ppm): 2.407 m (s, 3H, CH_3), 7.256–8.646 (m, 10H, Ar–H).

2.3. Crystallography

Suitable single crystal of BMBC was obtained by evaporation of acetone solution. The diffraction data were collected with a Bruker Smart Apex CCD area detector using a graphite monochromated Mo Kα radiation (λ = 0.71073 Å) at 20 °C. The structure was solved by using the program SHELXL and Fourier difference techniques, and refined by full-matrix least-squares method on F^2. All hydrogen atoms were added theoretically. The crystal and experimental data are shown in Table 1.

2.4. Quantum chemical calculations

The structure of BMBC was optimized by semiempirical density functional theory (DFT) using a B3LYP/6-31G(d)

Table 1
Crystal data and structure refinement for BMBC

Empirical formula	$C_{20}H_{13}N_3O_2$
Formula weight	327.33
Temperature (K)	293(2)
Wavelength (Å)	0.71073
Crystal system	Monoclinic
Space group	$P2_1/n$
Unit cell dimensions	$a = 6.4080(10)$ Å, $\alpha = 90°$; $b = 21.181(3)$ Å, $\beta = 100.126°$; $c = 11.5900(17)$ Å, $\gamma = 90°$
Volume (Å^3), Z	1548.6(4), 4
Density (calculated) (g/cm^3)	1.404
Absorption coefficient (mm^{-1})	0.093
F (0 0 0)	680
Crystal size (mm)	0.40 × 0.21 × 0.13
θ range for data collected (°)	1.92–26.07
Limiting indices	$-7 \le h \le 7$, $-26 \le k \le 25$, $-11 \le l \le 14$
Reflections collected	8842
Independent reflections	3053 ($R_{int} = 0.0217$)
Absorption correction	Semi-empirical from equivalents
Maximum and minimum transmission	0.9877 and 0.9634
Refinement method	Full-matrix least-squares on F^2
Data/restraints/parameters	3053/0/227
Goodness-of-fit on F^2	1.030
Final R indices [$I > 2\sigma(I)$]	$R1 = 0.0419$, $wR2 = 0.1068$
R indices (all data)	$R1 = 0.0545$, $wR2 = 0.1150$
Largest diff. peak and hole (Einstein Å^{-3})	0.179 and −0.203

basis set. The structural energy of BMBC was calculated at B3LYP/6-31G(d) levels. The structure optimization and energy calculations were performed with the GAUSSIAN 98 program.

3. Results and discussion

3.1. X-ray crystal structure

The crystal structure and packing diagram of BMBC are given in Figs. 1 and 2, respectively. The crystal data and experimental details are shown in Table 1. The selected bond lengths and bond angles of BMBC are listed in Table 2.

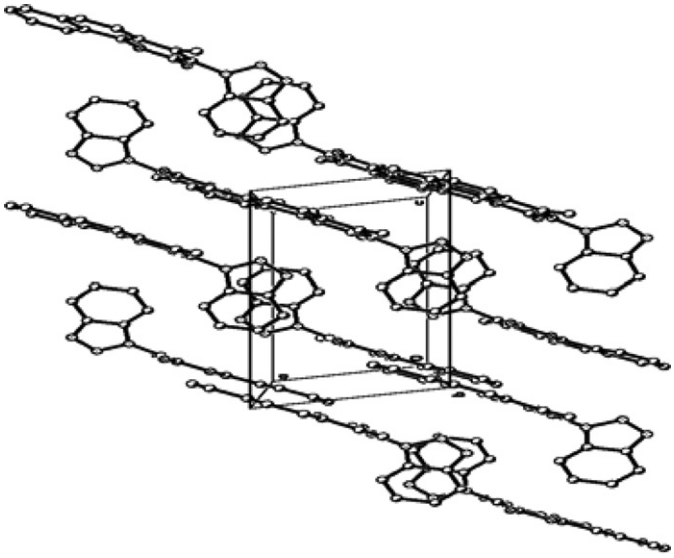

Fig. 2. Packing diagram along b-axis. H atoms are omitted for clarity.

Acceptable columnar-shaped crystals of BMBC suitable for X-ray analysis were obtained by slow evaporation of acetone solution, and the structure was measured by X-ray crystallography. The crystal of BMBC belongs to the monoclinic space group $P2_1/n$, $a = 6.4080$ (10) Å, $b = 21.181$ (3) Å, $c = 11.5900$ (17) Å, $\alpha = 90°$, $\beta = 100.126$ (2)°, $\gamma = 90°$, $U = 1548.6$ (4) Å^3, $Z = 4$, $D_c = 1.404$ g cm^{-3}, $p = 0.093$ mm^{-1}. As shown in Fig. 1, the benzotriazole skeleton is not coplanar with the benzocoumarin ring and the dihedral angle is 60.4°, attributed to steric interaction between 4-positioned methyl group and benzotriazole group.

The packing diagram for unit cell of BMBC was shown in Fig. 2. The benzotriazole group prevents the formation of a regular stacking arrangement of the molecules along c-axis, but they include the anti-parallel ABAB-type stacking and forming line chains along a-axis. The interplanar (A···B) distance is approximately 3.6 Å, which means weak intermolecular π–π stacking interaction between BMBC molecules in crystal lattice.

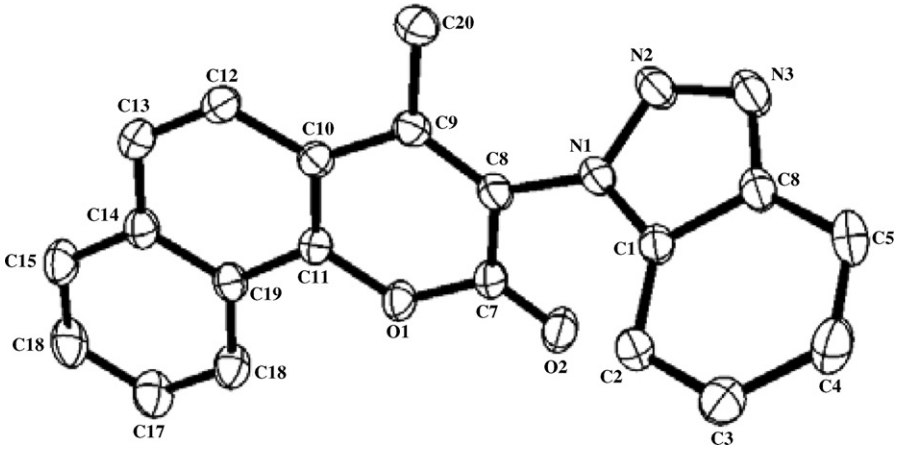

Fig. 1. Crystal structure of BMBC.

Table 2
Experimental and calculated structural parameters of BMBC molecule

Bond length (Å)	Experimental	Calculated	Bond angles (°)	Experimental	Calculated
C(1)–N(1)	1.3652(17)	1.3743	N(1)–C(1)–C(6)	104.17(12)	103.693
C(1)–C(6)	1.3907(18)	1.4079	N(1)–C(1)–C(2)	133.42(12)	134.366
C(1)–C(2)	1.3915(19)	1.4021	C(6)–C(1)–C(2)	122.40(13)	121.922
C(2)–C(3)	1.370(2)	1.3868	C(3)–C(2)–C(1)	116.19(13)	116.359
C(3)–C(4)	1.405(2)	1.4163	C(2)–C(3)–C(4)	121.98(15)	122.188
C(4)–C(5)	1.362(2)	1.3849	C(5)–C(4)–C(3)	121.62(15)	121.223
C(5)–C(6)	1.398(2)	1.4038	C(4)–C(5)–C(6)	117.35(14)	117.276
C(6)–N(3)	1.3791(19)	1.3814	N(3)–C(6)–C(1)	108.54(12)	108.760
C(7)–O(2)	1.2034(17)	1.2083	N(3)–C(6)–C(5)	131.01(13)	130.206
C(7)–O(1)	1.3687(16)	1.3872	C(1)–C(6)–C(5)	120.45(14)	121.031
C(7)–C(8)	1.453(2)	1.4647	O(2)–C(7)–O(1)	117.55(12)	117.987
C(8)–C(9)	1.3548(19)	1.3697	O(2)–C(7)–C(8)	126.16(13)	126.480
C(8)–N(1)	1.4249(17)	1.4139	O(1)–C(7)–C(8)	116.29(12)	115.520
C(9)–C(10)	1.4495(19)	1.4521	C(9)–C(8)–N(1)	123.40(12)	122.086
C(9)–C(20)	1.5007(19)	1.5050	C(9)–C(8)–C(7)	122.94(13)	122.569
C(10)–C(11)	1.3734(19)	1.3921	N(1)–C(8)–C(7)	113.66(12)	114.309
C(10)–C(12)	1.4246(19)	1.4294	C(8)–C(9)–C(10)	117.68(12)	118.318
C(11)–O(1)	1.3705(16)	1.3600	C(8)–C(9)–C(20)	122.62(13)	122.499
C(11)–C(19)	1.4199(19)	1.4250	C(10)–C(9)–C(20)	119.70(12)	119.182
C(12)–C(13)	1.357(2)	1.3685	C(11)–C(10)–C(12)	117.41(13)	117.860
C(13)–C(14)	1.419(2)	1.4257	C(11)–C(10)–C(9)	118.93(12)	118.778
C(14)–C(15)	1.414(2)	1.4173	C(12)–C(10)–C(9)	123.58(12)	123.361
C(14)–C(19)	1.4137(19)	1.4293	O(1)–C(11)–C(10)	121.81(12)	121.370
C(15)–C(16)	1.359(2)	1.3786	O(1)–C(11)–C(19)	114.72(11)	115.882
C(16)–C(17)	1.394(2)	1.4142	C(10)–C(11)–C(19)	123.47(12)	122.748
C(17)–C(18)	1.365(2)	1.3781	C(13)–C(12)–C(10)	121.20(13)	121.236
C(18)–C(19)	1.409(2)	1.4183	C(12)–C(13)–C(14)	121.28(13)	121.121
N(1)–N(2)	1.3672(16)	1.3879	C(15)–C(14)–C(19)	118.09(13)	118.524
N(2)–N(3)	1.2984(17)	1.2850	C(15)–C(14)–C(13)	122.74(13)	122.258
			C(19)–C(14)–C(13)	119.17(13)	119.218
			C(16)–C(15)–C(14)	120.90(15)	120.790
			C(15)–C(16)–C(17)	120.83(15)	120.375
			C(18)–C(17)–C(16)	120.11(15)	120.455
			C(17)–C(18)–C(19)	120.43(15)	120.108
			C(18)–C(19)–C(14)	119.59(13)	118.528
			C(18)–C(19)–C(11)	122.93(13)	122.436
			C(14)–C(19)–C(11)	117.45(12)	117.817
			C(1)–N(1)–N(2)	110.08(11)	109.479
			C(1)–N(1)–C(8)	127.84(11)	128.654
			N(2)–N(1)–C(8)	122.06(11)	121.846
			N(3)–N(2)–N(1)	108.50(12)	109.063
			N(2)–N(3)–C(6)	108.69(12)	108.997
			C(7)–O(1)–C(11)	122.05(11)	123.354

Symmetry transformations used to generate equivalent atoms.

3.2. Thermal property of BMBC

The TG and DTA measurements were performed in flowing drying nitrogen atmosphere at the heating rate of 10 °C/min on approximately 3.82 mg sample. The result of TG and DTA measurements of BMBC is shown in Fig. 3. From Fig. 3, it is shown that there is no endothermic behavior in the DTA curve and no mass loss in the TG curve up to 250 °C. It can be seen that the DTA curve shows an endothermic peak at 264 °C, but without mass loss in the TG curve. It indicates that the temperature is the melting point of the compound, which is in agreement with the result obtained by a melting point apparatus. At 345.6 and 583 °C two exothermic peaks were observed in the DTA curve, and corresponding to sharp weight losses in the TG curve, it shows

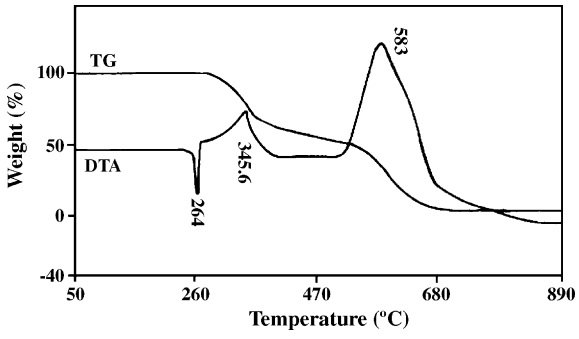

Fig. 3. TG-DTA of BMBC.

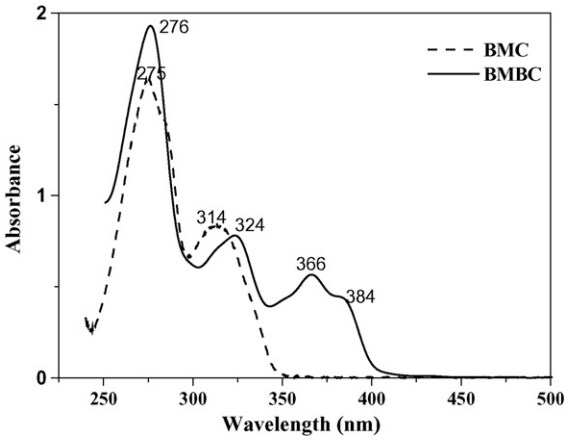

Fig. 4. UV–vis absorption spectra of BMC (- - -) and BMBC (—) in chloroform (5×10^{-5} mol/l).

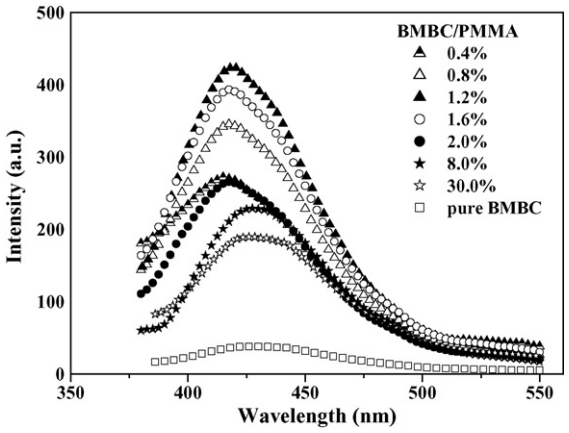

Fig. 6. The emission spectral features of BMBC in the BMBC/PMMA systems (C_{PMMA} = 15 mg/ml, λ_{ex} = 366 nm).

that the compound undergoes two large-stage decomposition processes.

3.3. Absorption and fluorescence of BMBC

UV–vis absorption spectra of BMBC in diluted chloroform solutions are given in Fig. 4. We can see that the absorption spectrum of BMBC shows absorptions at λ_{max} = 275, 325, 366 and 385 nm, respectively. Compared with 3-(1-benzotriazole)-4-methyl-coumarin (BMC) [16], an important feature of the absorption spectra of BMBC is shown that two absorption peaks were observed at 366 and 385 nm, which were absent in the spectra of BMC. The other feature is that the second absorption band at 324 nm was bathochromically shifted in BMBC compared to BMC in which the absorption band is at 314 nm, it is suggesting that the conjugation of benzocoumarin ring in BMBC is larger than that of coumarin skeleton in BMC. As a result, the red shift of absorption can possibly occur.

Fig. 5 shows the excitation and emission spectra of BMBC in dilute chloroform solution. From Figs. 4 and 5, it is shown that the shape of excitation spectrum of BMBC strongly resembles that of UV–vis absorption spectrum, and three intense excitation peaks were observed at 275, 325 and 366 nm, respectively. The compound exhibits bright blue emission with peak at 424 nm in dilute solution, but it was also found that sharp self-quenching and much broader emission band of the solid state brought about the compact piling of the solids was occurred, suggesting that the compound in the solid state has more intermolecular interaction than that in solution situation, and thus may lead to change of the emission band.

The emission peak of BMBC appeared at around 424 nm, which was red-shifted by about 39 nm with respect to that of BMC due to the larger conjugation of benzocoumarin ring in BMBC.

The photoluminescent behaviors of BMBC doped in poly (methyl methacrylate) (PMMA) were investigated detailedly as shown in Fig. 6. Mixed systems of BMBC with PMMA were prepared by dissolving these components with a certain weight ratios into acetone. The samples for photoluminescent spectroscopy were made by spin-coating the acetone solutions onto clean quartz substrates. It was found that the emission spectral features of BMBC in the BMBC/PMMA systems change with the weight ratios of the compound and PMMA. It is noticed that there is the strongest blue emission at about concentration of 1.2 wt% the compound. When the concentration was lower 1.2 wt%, the emission peak was located at around 420 nm, and the relative intensity increases gradually with increasing the weight ratio. When the concentration was higher than 1.2 wt%, the emission peak was shifted to longer wavelength, and the emission intensity was decreasing.

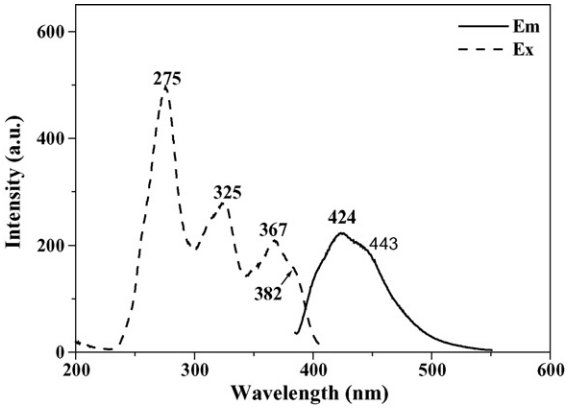

Fig. 5. Excitation (- - -) and emission (—) spectra of BMBC in dilute chloroform solutions at room temperature ($C = 5 \times 10^{-5}$ mol/l, λ_{ex} = 366 nm, λ_{em} = 424 nm).

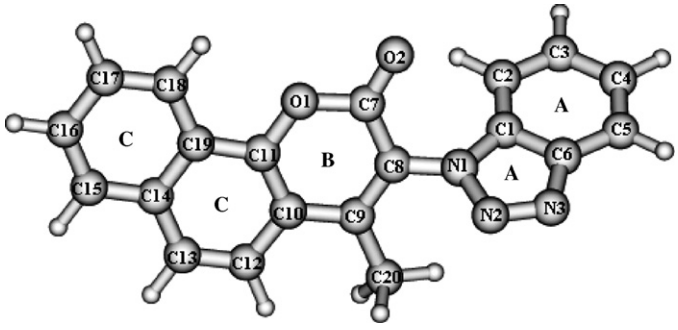

Fig. 7. B3LYP/6-31G(d)-optimized structure of BMBC.

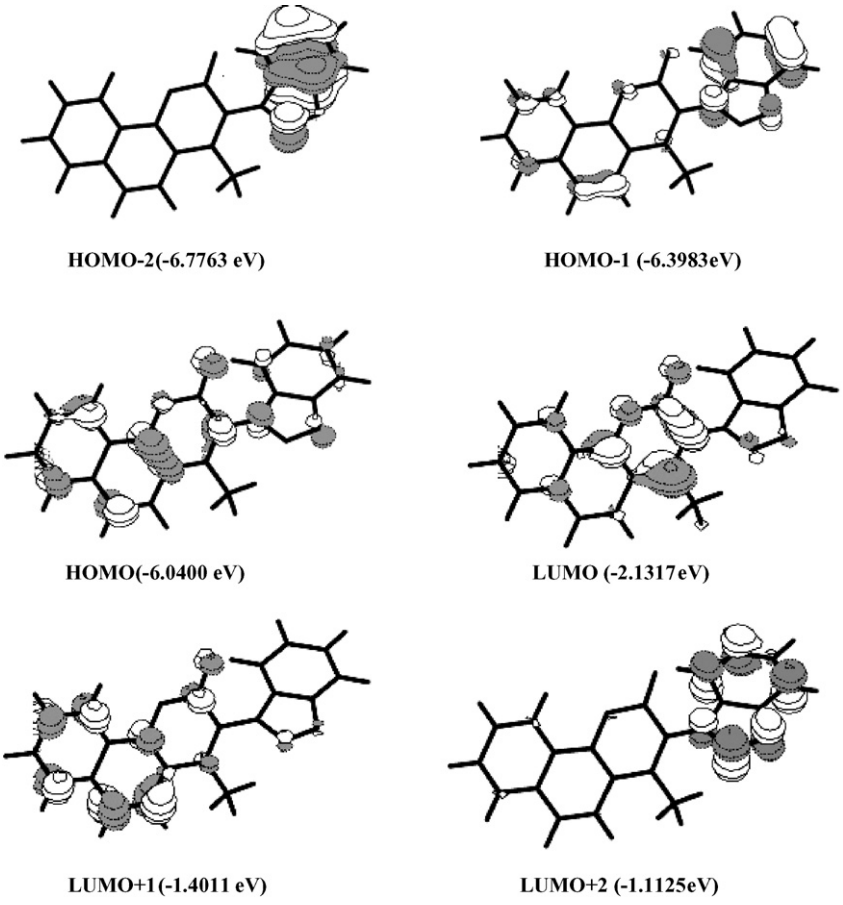

Fig. 8. Frontier molecular orbitals of compound BMBC.

3.4. Quantum chemical calculations

The structure of BMBC obtained from B3LYP/6-31G(d) calculations is shown in Fig. 7, indicating that the DFT optimized structure is close to the crystal structure.

B3LYP/6-31G(d) optimized geometrical data of BMBC were obtained. It was found that the B3LYP/6-31G(d) optimized structure of BMBC is in good agreement with the X-ray crystallographic data as listed in Table 2. The results show that the average discrepancy of bond lengths between theoretical and experimental data is less than ±0.02 Å, and the average discrepancy of bond angles is less than ±2°. Therefore, the results using density functional theory (DFT) at B3LYP/6-31G(d) level is creditable. The HOMO and LUMO levels of BMBC were deduced using DFT method as shown in Fig. 8, which is essential for deducing its S_0 and S_1 states. From Fig. 8, it can be seen that the HOMO of BMBC is −6.0400 eV and the LUMO is −2.1317 eV. The electron density of the HOMO is localized in the whole molecular skeleton, and the electron density of the LUMO is distributed mainly at the coumarin ring. The energy gap between HOMO and LUMO is about 3.9083. Compared with BMC [16], the bandgap energy of BMBC is less than that of BMC, suggesting that the conjugation of benzocoumarin ring in BMBC is larger than that of coumarin skeleton in BMC.

The UV–vis absorption spectra of BMBC were also calculated using time-dependent density functional theory (TD-DFT) at the same level. Table 3 lists the data of the experimental and calculated λ_{max} (nm) for the lower-lying singlet state of BMBC. This strategy leads to an average discrepancy of 30 nm between theoretical and experimental λ_{max} due to several influencing factors, such as solvent effect and intermolecular interaction, etc. It has been found that the lowest energy absorption at 385 nm

Table 3
Absorption spectra data of BMBC

Transition character	OSC[a]	$\lambda_{max, cal.}$ (nm)	$\lambda_{max, exp.}$ (nm)[b]	Transition feature
HOMO → LUMO	0.2957	358.03	385	$\pi \rightarrow \pi^*$
HOMO-1 → LUMO	0.0177	338.00	367	$\pi \rightarrow \pi^*$
HOMO-2 → LUMO; HOMO → LUMO+1	0.0246	306.39	325	$\pi \rightarrow \pi^*$
HOMO-1 → LUMO + 1; HOMO → LUMO + 1; HOMO-1 →LUMO + 2	0.3778	265.42	275	$\pi \rightarrow \pi^*$

[a] Oscillator strength coefficients (*f*).
[b] λ_{max} in chloroform solvent.

(calculated value 358.03 nm) is due to the electronic $\pi \rightarrow \pi^*$ transition from the HOMO to the LUMO, and it is arisen from the charge transfer transition from molecular segment C to molecular segment B (Figs. 7 and 8). The second transition occurring at 367 nm (calculated value 338.00 nm) is an excitation from the HOMO-1 to the LUMO, and it is arisen from the charge transfer from molecular segment A to molecular segment B. The calculation outcomes have shown that the UV absorption spectrum of the compound calculated by TD-DFT method is in good agreement with the experimental data, and accurately explain the experimental results.

4. Conclusions

The novel coumarin derivative, BMBC, was synthesized and confirmed by means of element analysis, ^{1}H NMR, FT-IR and UV–vis absorption spectra, TG-DTA and single crystal X-ray crystallography. Its structure was studied both experimentally and theoretically. The compound has high thermal stability, and exhibites bright blue emission with peak at 424 nm in dilute solution. It was found that the emission spectral features of BMBC doped in PMMA change with the weight ratios of the compound and PMMA, and the strongest blue emission is at about concentration of 1.2 wt% the compound. The HOMO and LUMO levels of BMBC were deduced using DFT method, and the TD-DFT approach has been applied to the study of the UV–vis spectrum of BMBC and the calculation outcomes are in good agreement with the experimental data, and accurately explain the experimental results.

Supplementary material

The crystallographic data (excluding structure factors) of BMBC has been deposited with the Cambridge Crystallographic Center as supplementary publication no. CCDC 611438.

Acknowledgement

This work was supported by ‘Qing Lan’ talent engineering funds (QL-05-23A) by Lanzhou Jiaotong University.

References

[1] K.H. Drexhage, in: F.P. Schäfer (Ed.), Topics in Applied Physics Dye Lasers, vol. 1, Springer, Berlin, 1973.
[2] G. Jones, W.R. Jackson, C. Choi, W.R. Bergmark, J. Phys. Chem. 89 (1985) 294.
[3] T. Hiroshi, O. Yosho, I. Juzo, I. Masato, T. Atsushi, Jpn. Kokai Tokkyo Koho, 1990. CODEN: JKXXAF JP 02126241 A2 19900515 Heisei.
[4] H.E. Patel, K.R. Desai, J. Inst. Chem. 68 (1996) 78.
[5] R.P. Haugland, Handbook of Fluorescent Probes and Research Chemicals, Molecular Probes, Eugene (OR), 1994–1996.
[6] H. Schwander, P. Hendrix, in: Y.S. Yamamoto (Ed.), Ullmann’s Encyclopedia of Industrial Chemistry, vol. A11, 5th ed., VCH, Weinheim, 1988, p. 280.
[7] H.K. Arora, A.R. Aggarwal, R.P. Singh, Indian J. Chem. 21A (1982) 844.
[8] O.S. Wolfbeis, E. Koller, P. Hochmuth, Bull. Chem. Soc. Jpn. 58 (1985) 731.
[9] C.W. Tang, S.A. VanSlyke, C.H. Chen, J. Appl. Phys. 65 (1989) 3610.
[10] C.T. Chen, C.L. Chiang, Y.C. Lin, L.H. Chan, C.H. Huang, Z.W. Tsai, C.T. Chen, Org. Lett. 5 (2003) 1261.
[11] M.T. Lee, C.K. Yen, W.P. Yang, H.H. Chen, C.H. Liao, C.H. Tsai, C.H. Chen, Org. Lett. 6 (2004) 1241.
[12] S.A. Swanson, G.M. Wallraff, J.P. Chen, W.J. Zhang, L.D. Bozano, K.R. Carter, J.R. Salem, R. Villa, J.C. Scott, Chem. Mater. 15 (2003) 2305.
[13] J. Kido, K. Hongawa, K. Okuyama, K. Nagai, Appl. Phys. Lett. 64 (1994) 815.
[14] C.-C. Wu, J.C. Sturm, R.A. Register, J. Tian, E.P. Dana, M.E. Thompson, IEEE Trans. Electron. Dev. 44 (1997) 1269.
[15] H.P. Zheng, R.F. Zhang, F. Wu, W.J. Tian, J.C. Shen, Synth. Met. 100 (1999) 291.
[16] T.Z. Yu, Y.L. Zhao, D.W. Fan, J. Mol. Struct. 791 (1–3) (2006) 18.